An unprecedented polyhydroxycarboxylic acid ligand bridging multi-Eu^{III} incorporated tellurotungstate and its luminescence properties

Yan Zhang,[a] Dan Wang,[a] Baoxing Zeng,[a] Lijuan Chen,*,[a] Junwei Zhao,*,[a] and Guo-Yu Yang*,[b]

[a] *Henan Key Laboratory of Polyoxometalate Chemistry, College of Chemistry and Chemical Engineering, Henan University, Kaifeng, Henan 475004, China*

[b] *MOE Key Laboratory of Cluster Science, School of Chemistry, Beijing Institute of Technology, Beijing 100081, China*

Electronic Supplementary Information

represent **1a** polyanions and turquoise spheres represent K2$^+$ cations.

Fig. S11 (a) IR spectra of **1**, K_2TeO_3 and H_6glu. (b) The TG curve of **1**.

Fig. S12 The solid-state excitation spectrum of **1** obtained by monitoring the emission at 470 nm (The emission at 470 nm is attributed to the $^3T_{1u}\rightarrow{}^1A_{1g}$ transition of the O→W LMCT of TT fragments, which can be obviously observed from the TRES profiles of **1** in Fig. 5e and 5g).

Fig. S13 (a) The emission spectrum of **1** in aqueous solution (C = 1.00 mM) under excitation at 394 nm. (b) The excitation spectrum of **1** in aqueous solution (C = 1.00 mM) taken by monitoring the strongest emission at 614 nm. (c) The lifetime decay curve of **1** obtained by monitoring the strongest emission at 614 nm.

Fig. S14 (a) The ^{125}Te NMR spectrum of **1** collected for the first time in D_2O solution. (b) The ^{125}Te NMR spectrum of **1** collected for the second time in D_2O solution.

Fig. S15 The simulated ESI–MS peaks of (a) $\{[Eu_4(H_2O)_8W_6(H_6glu)_4O_{12}(B\text{-}\alpha\text{-}TeW_9O_{33})_4]\}$, (b) $\{Na[Eu_4(H_2O)_{10}W_6(H_6glu)_4O_{12}(B\text{-}\alpha\text{-}TeW_9O_{33})_4]\}$, (c) $\{K_2[Eu_4(H_2O)_4W_6(H_6glu)_4O_{12}(B\text{-}\alpha\text{-}TeW_9O_{33})_4]\}$, (d) $\{K_2[Eu_4(H_2O)_{12}W_6(H_6glu)_4O_{12}(B\text{-}\alpha\text{-}TeW_9O_{33})_4]\}$, (e) $\{K_2Na[Eu_4(H_2O)_{14}W_6(H_6glu)_4O_{12}(B\text{-}\alpha\text{-}TeW_9O_{33})_4]\}$ fragments.

Fig. S16 (a) Evolution of FL emission spectra of **1** in aqueous solution for 96 h. (b) The emission spectrum of $Eu(NO_3)_3\cdot 6H_2O$ in distilled water (λ_{ex} = 394 nm). (c) Evolution of UV spectra of **1** in aqueous solution for 96 h.

Fig. S17 Lifetime decay curves of **1** in aqueous solution in different times.

Fig. S18 (a) Emission spectra of the **1**-sensor with addition of different metal cations. (b) Emission spectra of the **1**-sensor in the present of the Cu^{2+} ion and other metal ions. (c) The emission spectra of the **1**-sensor in the presence of different anions.

Fig. S19 ESI–MS spectrum of **1** in aqueous solution and the ESI-MS spectrum of the solution containing **1**, Cu^{2+} and Cys.

Fig. S20 (a) IR spectra of **1** grown from aqueous solution and **1** grown from the Cu^{2+}-containing aqueous solution. (b) PXRD patterns of **1** grown from aqueous solution and **1** grown from the Cu^{2+}-containing aqueous solution.

Fig. S21 XPS spectra of the crystals grown in the solution with and without Cu^{2+} ion.

Fig. S22 (a) Emission spectra of the sensor platform in the present of 0.001 mM Cu^{2+} ion in different temperature ($C_{\mathbf{1}}$ = 1 mg / mL, λ_{ex} = 394 nm). (b) Emission spectra of the solution of **1** in different temperature ($C_{\mathbf{1}}$ = 1 mg / mL, λ_{ex} = 394 nm).

Fig. S23 Evolution of emission spectra for the Cu^{2+}-quenching system based on **1** with addition of different aminoacids. [Conditions: 1.00 mg **1** was added to a series of 1.00 mL solutions simultaneously containing 4.00×10^{-2} mM Cu^{2+} ion and 0.10 mM aminoacids; Aminoacids include polar neutral aminoacid cysteine (Cys), glycine (Gly) and threonine (Thr), polar negative charged aminoacid glutamic acid (Glu), polar positively charged aminoacid lysine (Lys), respectively.]

Fig. S24 ESI–MS spectrum of **1** in aqueous solution and the ESI-MS spectrum of the solution containing **1**, Cu^{2+} and Cys.

Table S1. Crystallographic data and structure refinements for **1**.

	1
Empirical formula	$K_{14}H_{170}Eu_4W_{42}O_{236}C_{24}Te_4$
Formula weight	13622.93
Crystal system	Hexagonal
Space group	$P6_1$
a, Å	44.9573(17)
b, Å	44.9573(17)
c, Å	25.3111(9)
α, deg	90
β, deg	90
γ, deg	120
V, Å^{-3}	44304(4)
Z	6
μ, mm^{-1}	17.798
F(000)	36216
T, K	296(2)
Limiting indices	$-53 \le h \le 45$
	$-53 \le k \le 53$
	$-30 \le l \le 30$
Reflections collected/unique	236689 / 51926
R_{int}	0.0769
R_{sigma}	0.0819
Data/restrains/parameters	51926 / 122 / 2345
GOF on F^2	1.039
R_1, wR_2 ($I>2\sigma(I)$)^a	0.0408, 0.0857
R_1, wR_2 (all data)	0.0607, 0.0902

Table S2. Selected assignments of negative charge peaks for **1** in the range of 1500–4000 m/z.

m/z (obs)	z	Assignment	m/z (calc)
1510.32	8–	$\{[Eu_4(H_2O)_8W_6(H_6glu)_4O_{12}(B\text{-}\alpha\text{-}TeW_9O_{33})_4]\}$	1511.10
1734.27	7–	$\{Na[Eu_4(H_2O)_{10}W_6(H_6glu)_4O_{12}(B\text{-}\alpha\text{-}TeW_9O_{33})_4]\}$	1736.85
2017.87	6–	$\{K_2[Eu_4(H_2O)_4W_6(H_6glu)_4O_{12}(B\text{-}\alpha\text{-}TeW_9O_{33})_4]\}$	2015.79
2040.52	6–	$\{K_2[Eu_4(H_2O)_{12}W_6(H_6glu)_4O_{12}(B\text{-}\alpha\text{-}TeW_9O_{33})_4]\}$	2039.80
2460.27	5–	$\{K_2Na[Eu_4(H_2O)_{14}W_6(H_6glu)_4O_{12}(B\text{-}\alpha\text{-}TeW_9O_{33})_4]\}$	2459.56

Table S3. The ratios of $I(^5D_0 \rightarrow {}^7F_2)$ / $I(^5D_0 \rightarrow {}^7F_1)$ for $Eu(NO_3)_3 \cdot 6H_2O$ in aqueous solution and the ratios of $I(^5D_0 \rightarrow {}^7F_2)$ / $I(^5D_0 \rightarrow {}^7F_1)$ for **1** in aqueous solution at different times.

	$I(^5D_0 \rightarrow {}^7F_2)$ / 10^3	$I(^5D_0 \rightarrow {}^7F_1)$ / 10^3	ratio

$Eu(NO_3)_3{\cdot}6H_2O$	51.07	93.06	0.55
1 (0 h)	96.37	29.98	3.21
1 (2 h)	89.00	28.11	3.17
1 (4 h)	74.11	23.58	3.14
1 (6 h)	66.84	21.13	3.16
1 (8 h)	60.15	19.25	3.12
1 (10 h)	58.25	17.74	3.28
1 (24 h)	76.31	24.42	3.00
1 (48 h)	86.57	27.17	3.19
1 (72 h)	87.80	28.52	3.08
1 (96 h)	89.32	28.57	3.13

Table S4. Luminescence decay lifetimes for **1** in aqueous solution at different times.

	τ_1/μs	**A_1**	**Percentage /%**	**τ_2/μs**	**A_2**	**Percentage /%**	**τ/μs**	**χ^2**
0 h	100.00	3.10	0.08	396.73	990.79	99.92	396.50	1.022
2 h	10.11	83.20	0.22	398.34	936.90	99.78	397.47	1.149
4 h	45.89	29.18	0.34	399.93	981.48	99.66	398.72	0.987
6 h	51.76	35.24	0.47	393.30	976.51	99.53	391.69	1.035
8 h	23.11	43.51	0.63	394.87	953.31	99.37	393.88	1.002
10 h	100.00	58.37	1.5	106.10	945.68	98.50	105.76	1.086
24 h	65.03	47.02	0.83	398.50	916.02	99.17	395.72	0.986
48 h	9.93	82.57	0.65	393.74	1011.65	99.35	392.95	1.072
72 h	40.39	43.36	0.46	394.51	955.90	99.54	392.87	0.914
96 h	100.00	16.73	0.46	395.34	922.83	99.54	394.00	1.029
120 h	12.81	28.24	0.02	390.77	976.97	99.98	390.41	1.002
148 h	41.63	3.64	0.04	390.50	984.03	99.96	390.36	1.096
172 h	76.36	19.20	65.45	391.05	939.73	38.65	398.80	1.013

Table S5. The K_{SV} results of monitoring the Cu^{2+} cation in aqueous solution.

Fluorescnece reagents	**The concentration of Cu^{2+} cation (mM)**	**Value of Ksv (mM^{-1})**	**Ref.**

MOF	0.10	7.67	[9]
MOF	0.75	10	[10]
1	0.08	123.17	Our work

Table S6. The standard deviation for the FL sensor based on **1**.

Blank Readings (only 1 mg mL^{-1} **1**-based probe)	***I***(FL Intensityof the main emission peak at 614 nm)	**AVG.** (Average value of *I*)	**AVG. / *I***	**Standard Deviation (*s*)**
Reading 1	95886.72	95900.54	1.0001	3.60×10^{-4}
Reading 2	95875.23		1.0002	
Reading 3	95939.67		0.9996	

Table S7. The *LOD* calculation for the sensor based on **1** to detect the Cu^{2+} cation.

Slope from Graph (*k*)	122.6591	mM^{-1}
LOD (3*k* / *s*)	8.8185×10^{-6}	mM

Table S8. The standard deviation for the Cu^{2+}-quenching system based on **1** to detect Cys.

Blank readings (1 mg mL^{-1} POM-based probe + 0.04 mM Cu^{2+})	***I*** (FL Intensityof the main emission peak at 614 nm)	**AVG.** (Average value of *I*)	***I* / AVG.**	**Standard deviation (*s*)**
Reading 1	15620.58	15592.80	1.0018	1.96×10^{-3}
Reading 2	15597.59		1.0003	
Reading 3	15560.23		0.9979	

Table S9. The *LOD* calculation for the Cu^{2+}-quenching system based on **1** to detect Cys.

Slope (*k*)	33.8079	mM^{-1}
Detection limit (3*k* / *s*)	1.7456×10^{-4}	mM

Table S10. Summary of lifetimes fitting parameters of the Cu^{2+}-quenching system based on **1** with addition of Cys by monitoring the strongest emission at 614 nm under excitation at 394 nm.

C_{Cys}	τ_1/ μs	A_1	τ_2/ μs	A_2	τ^* / μs	X^2
0.02	10.00	17.77	77.93	10.24	64.99	1.098
0.04	11.51	16.90	92.88	9.03	77.56	1.128
0.05	20.00	13.15	126.07	6.54	100.42	1.366
0.06	20.00	12.83	126.81	6.40	101.15	1.304
0.07	100.00	491.61	154.28	500.71	133.17	1.111
0.08	11.21	50.83	215.14	12.01	178.29	1.089
0.09	100.00	73.63	239.42	79.77	200.62	1.042
0.10	100.00	63.95	252.58	69.64	211.90	1.119
0.11	100.00	108.02	283.77	117.72	238.87	1.201
0.12	100.00	80.66	331.64	84.48	279.86	0.978
0.13	100.00	67.32	392.99	37.39	300.93	0.993
0.14	50.69	70.76	367.59	36.98	301.43	0.936
0.15	100.00	66.47	380.00	63.94	319.85	0.904
0.16	47.72	70.71	393.66	32.36	321.22	1.033
0.18	100.00	65.80	388.10	62.82	326.87	1.026

0.20	100.00	65.76	388.28	327.15	327.15	1.077

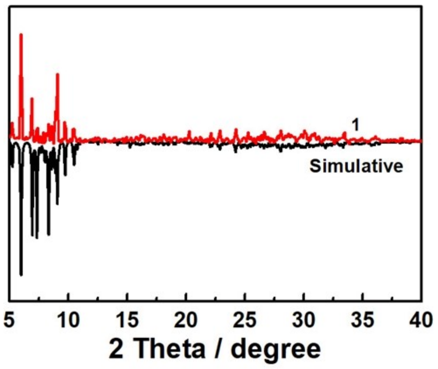

Fig. S1 Comparison of the PXRD pattern of **1** and its single-crystal XRD pattern.

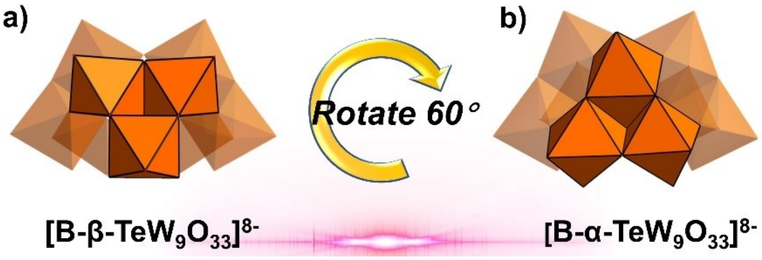

Fig. S2 The transformation relation between (a) [B-β-TeW_9O_{33}]$^{8-}$ and (b) [B-α-TeW_9O_{33}]$^{8-}$ fragments.

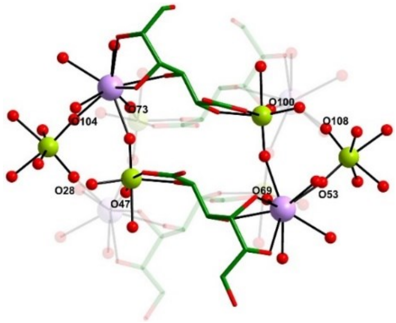

Fig. S3 View of the linking mode of Eu1 and W6, Eu2 and W2, Eu3 and W4, Eu4 and W3 centers in **1b**.

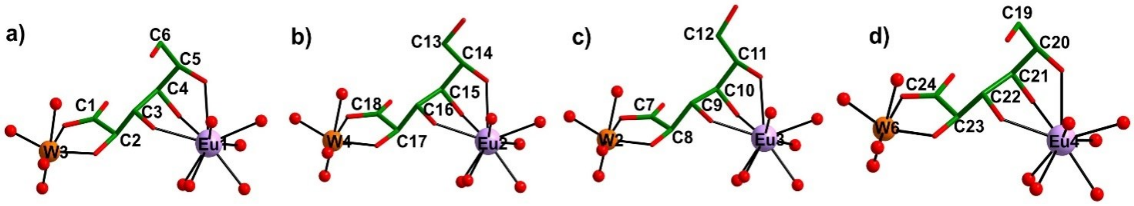

Fig. S4 (a−d) Four [$Eu(H_2O)W(H_2glu)O_2$]$^+$ entities highlighting flexible polyhydroxycarboxylic coordination mode of H_2glu^{4-} ligands.

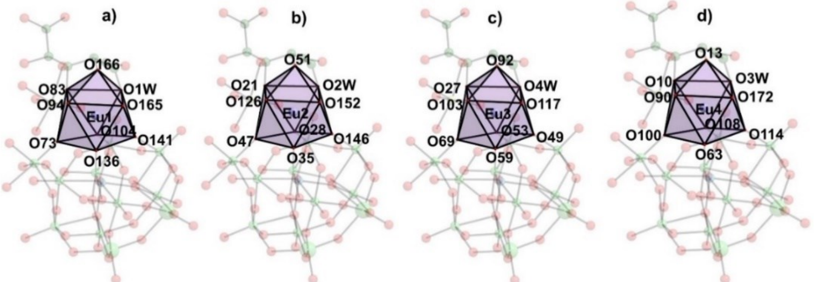

Fig. S5 (a−d) The distorted monocapped square antiprismatic geometries of four Eu^{3+} ions.

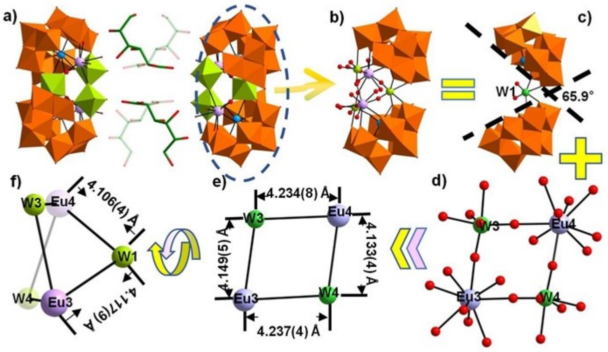

Fig. S6 (a) The combination between two $[Eu_2(H_2O)_2W_3O_6(B\text{-}\alpha\text{-}TeW_9O_{33})_2]^{4-}$ subunits and four H_2glu^{4-} linkers. (b) The dimeric $[Eu_2(H_2O)_2W_3O_6(B\text{-}\alpha\text{-}TeW_9O_{33})_2]^{4-}$ subunit containing W3, W4, Eu3 and Eu4 centers. (c) The openmouthed $[Te_2W_{19}O_{68}]^{8-}$ segment containing W1 bridge. (d) Top view of the tetra-nuclear $[Eu_2(H_2O)_2W_2O_4]^{10+}$ cluster constructed by W3, W4, Eu3 and Eu4 atoms. (e) The simplified view of the $[Eu_2(H_2O)_2W_2O_4]^{10+}$ cluster. (f) Side view of the simplified $[Eu_2(H_2O)_2W_3O_6]^{12+}$ cluster.

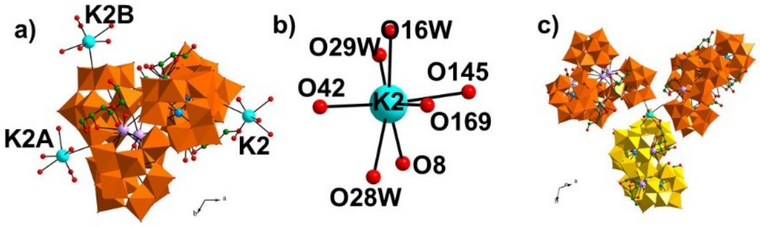

Fig. S7 (a) Each **1a** linking to three $K2^+$. The atoms with the suffixes A and B are generated by symmetry operations. A: −1+y, −x+y, −0.16667+z; B: −y, 1+x−y, 0.33333+z. (b) The distorted pentagonal bipyramid coordination environment of $K2^+$. (c) The connection motif of each $K2^+$ linking to three **1a**.

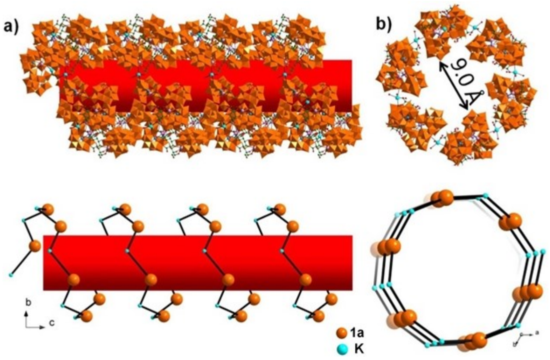

Fig. S8 (a) The right-handed helical channel A viewed along the *a* axis. (b) The right-handed helical channel A viewed along the *c* axis. Color code: yellow spheres represent **1a** polyanions and turquoise spheres represent $K2^+$ cations.

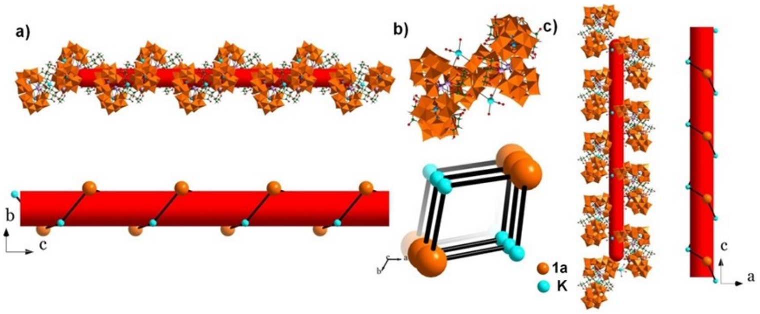

Fig. S9 (a) The left-handed helical channel B viewed along the *a* axis. (b) The left-handed helical channel B viewed along the *c* axis. (c) The helical channel B viewed along the *b* axis. Color code: yellow spheres represent **1a** polyanions and turquoise spheres represent K2⁺ cations.

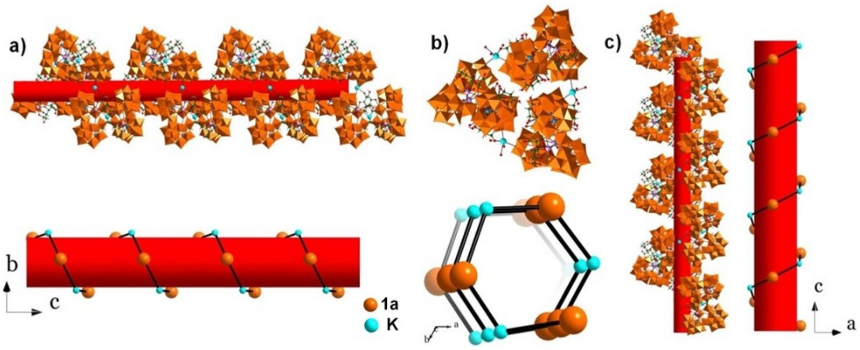

Fig. S10 (a) The right-handed helical channel C viewed along the *a* axis. (b) The right-handed helical channel C viewed along the *c* axis. (c) The right-handed helical channel C viewed along the *b* axis. Color code: yellow spheres represent **1a** polyanions and turquoise spheres represent K2⁺ cations.

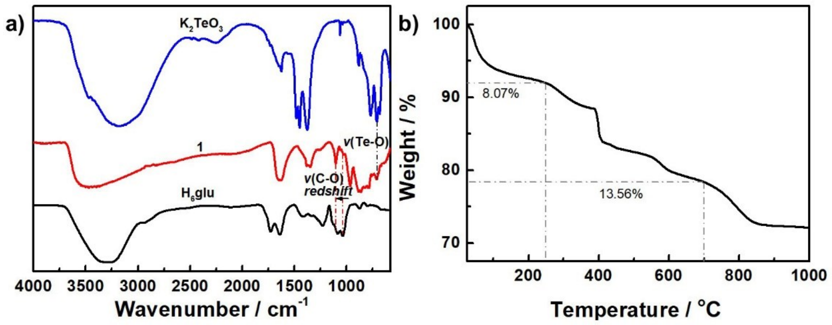

Fig. S11 (a) IR spectra of **1**, K_2TeO_3 and H_6glu. (b) The TG curve of **1**.

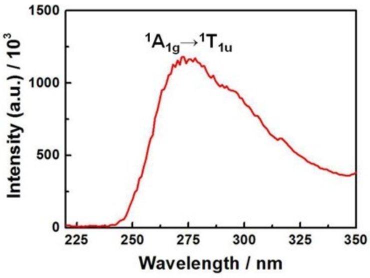

Fig. S12 The solid-state excitation spectrum of **1** obtained by monitoring the emission at 470 nm (The emission at 470 nm is attributed to the $^3T_{1u}\rightarrow{}^1A_{1g}$ transition of the O→W LMCT of TT fragments, which can be obviously observed from the TRES profiles of **1** in Fig. 5e and 5g).

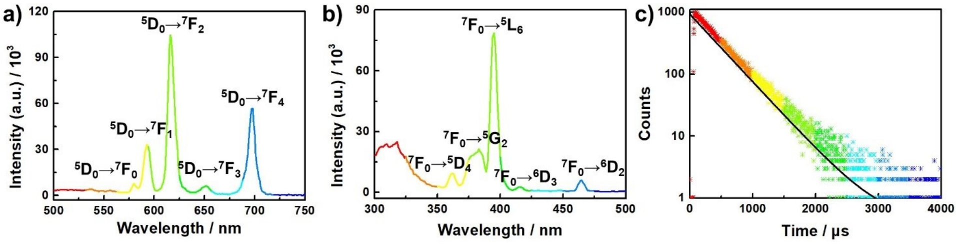

Fig. S13 (a) The emission spectrum of **1** in aqueous solution (C = 1.00 mM) under excitation at 394 nm. (b) The excitation spectrum of **1** in aqueous solution (C = 1.00 mM) taken by monitoring the strongest emission at 614 nm. (c) The lifetime decay curve of **1** obtained by monitoring the strongest emission at 614 nm.

As can be seen from Fig. S13a, the emission spectrum of **1** in aqueous solution shows five obvious characteristic emission bands at 579, 594, 614, 650 and 701 nm, which are attributed to the $^5D_0\rightarrow{}^7F_0$, $^5D_0\rightarrow{}^7F_1$, $^5D_0\rightarrow{}^7F_2$, $^5D_0\rightarrow{}^7F_3$

and $^5D_0 \rightarrow {}^7F_4$ transitions of the Eu^{3+} ion, respectively.[1] The excitation spectrum of **1** was recorded by monitoring the most intense emission peak at 614 nm, which shows five peaks at 362, 379, 394, 415 and 465 nm corresponding to the $^7F_0 \rightarrow {}^5D_4$, $^7F_0 \rightarrow {}^5G_2$, $^7F_0 \rightarrow {}^5L_6$, $^7F_0 \rightarrow {}^5D_3$ and $^7D_0 \rightarrow {}^5D_2$ transitions of the Eu^{3+} ion, respectively (Fig. S13b).[1] The lifetime decay curve of **1** was obtained by monitoring the most intense emission at 614 nm (Fig. S13c), which obeys a second-order exponential function $I = A_1\exp(-t/\tau_1) + A_2\exp(-t/\tau_2)$ (where τ_1 and τ_2 are fast and slow components of the FL lifetimes and A_1 and A_2 are pre-exponential factors). The fitting lifetimes are τ_1 = 100.00 μs (0.03 %) and τ_2 = 404.06 μs (99.97 %) and the pre-exponential factors are A_1 = 64.35 and A_2 = 59.44. Therefore, the average decay time (τ^*) can be determined by using the formula $\tau^* = (A_1\tau_1^2 + A_2\tau_2^2)/(A_1\tau_1 + A_2\tau_2)$, the average lifetime is calculated to be 339.81 μs.

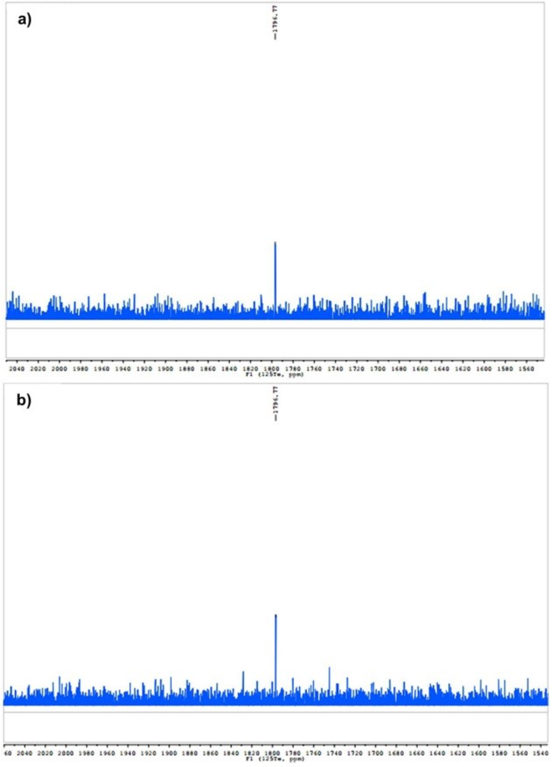

Fig. S14 (a) The ^{125}Te NMR spectrum of **1** collected for the first time in D_2O solution. (b) The ^{125}Te NMR spectrum of **1** collected for the second time in D_2O solution.

We have collected the ^{125}Te NMR spectra of **1** in D_2O solution twice, and both ^{125}Te NMR spectra exhibit almost the same characteristic signal at $\delta = -1796.77$ ppm in the range of 1580−2040 ppm, which corresponds to the Te^{IV} centers in the trivacant Keggin $[B\text{-}\alpha\text{-}TeW_9O_{33}]^{8-}$ fragments in **1**. The low signal intensity is due to the low content of Te^{IV} (3.75 wt%) in the structure of **1**.

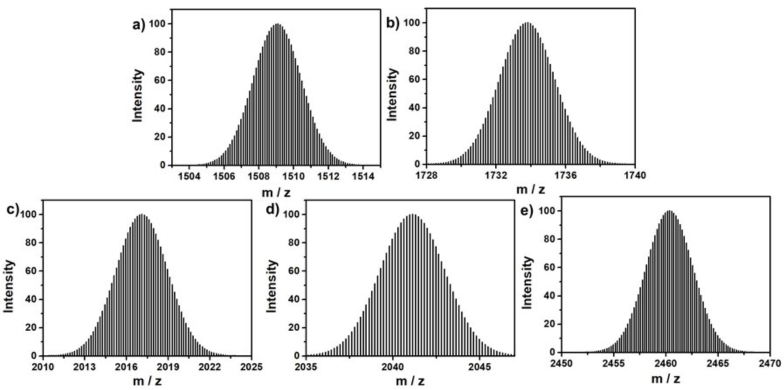

Fig. S15 The simulated ESI–MS peaks of (a) $\{[Eu_4(H_2O)_8W_6(H_6glu)_4O_{12}(B\text{-}\alpha\text{-}TeW_9O_{33})_4]\}$, (b) $\{Na[Eu_4(H_2O)_{10}W_6(H_6glu)_4O_{12}(B\text{-}\alpha\text{-}TeW_9O_{33})_4]\}$, (c) $\{K_2[Eu_4(H_2O)_4W_6(H_6glu)_4O_{12}(B\text{-}\alpha\text{-}TeW_9O_{33})_4]\}$, (d) $\{K_2[Eu_4(H_2O)_{12}W_6(H_6glu)_4O_{12}$

(B-α-TeW_9O_{33})$_4$]}, (e) {$K_2Na[Eu_4(H_2O)_{14}W_6(H_6glu)_4O_{12}$(B-α-$TeW_9O_{33})_4$]} fragments.

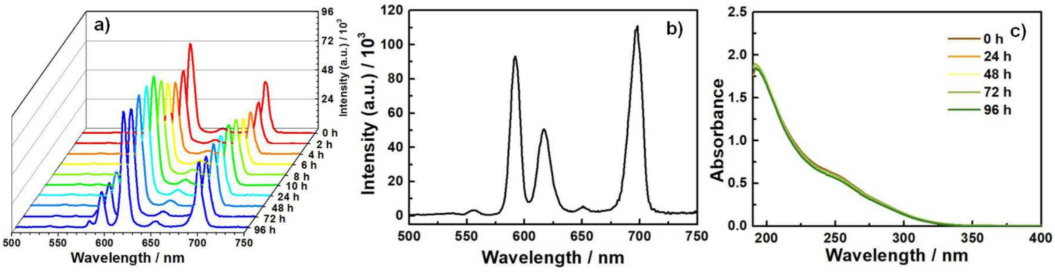

Fig. S16 (a) Evolution of FL emission spectra of **1** in aqueous solution for 96 h. (b) The emission spectrum of $Eu(NO_3)_3 \cdot 6H_2O$ in distilled water (λ_{ex} = 394 nm). (c) Evolution of UV spectra of **1** in aqueous solution for 96 h.

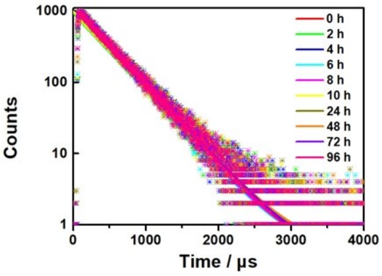

Fig. S17 Lifetime decay curves of **1** in aqueous solution in different times.

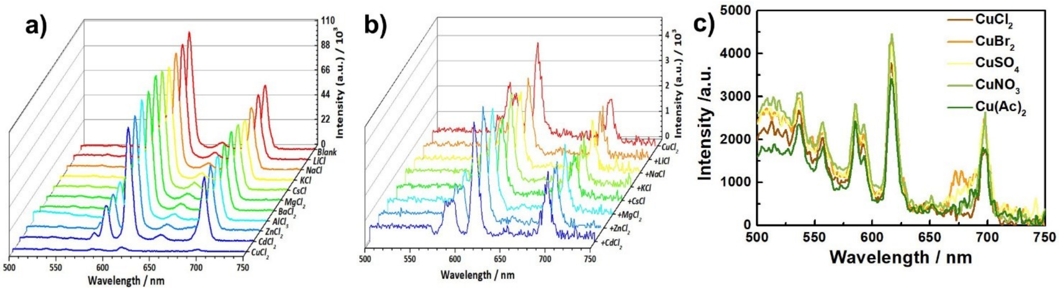

Fig. S18 (a) Emission spectra of the **1**-sensor with addition of different metal cations. (b) Emission spectra of the **1**-sensor in the present of the Cu^{2+} ion and other metal ions. (c) The emission spectra of the **1**-sensor in the presence of different anions.

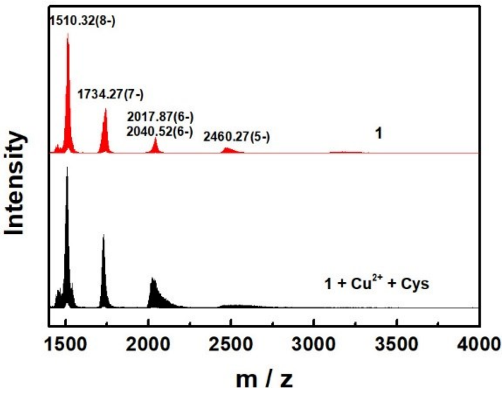

Fig. S19 ESI–MS spectra of **1** in aqueous solution and the ESI-MS spectrum of the solution containing **1**, Cu^{2+} and Cys.

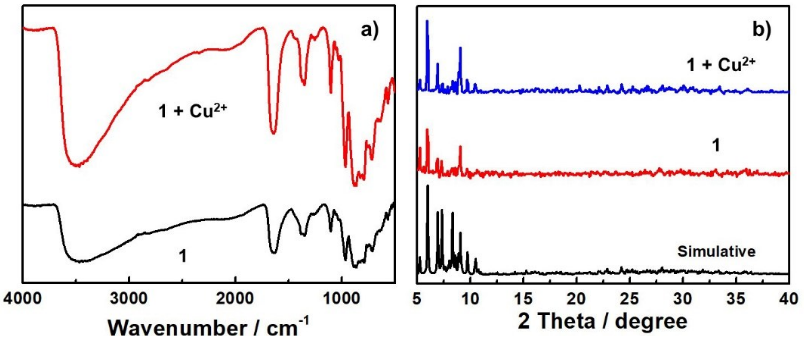

Fig. S20 (a) IR spectra of **1** grown from aqueous solution and **1** grown from the Cu^{2+}-containing aqueous solution. (b) PXRD patterns of **1** grown from aqueous solution and **1** grown from the Cu^{2+}-containing aqueous solution.

In order to testify that the POA skeleton structure of **1** can be retained during detecting the Cu^{2+} ion, before evaporating the reaction solution to crystallize **1**, we added 852.4 mg $CuCl_2\cdot 2H_2O$ (100.0 mM) into the reaction solution. Gratifyingly, colorless crystals with the original rod-like appearance were still obtained. IR and PXRD patterns of the crystals grown from the solution containing Cu^{2+} ions are well consistent with the original data, suggesting that the POA skeleton structure of **1** doesn't vary during detecting the Cu^{2+} ion.

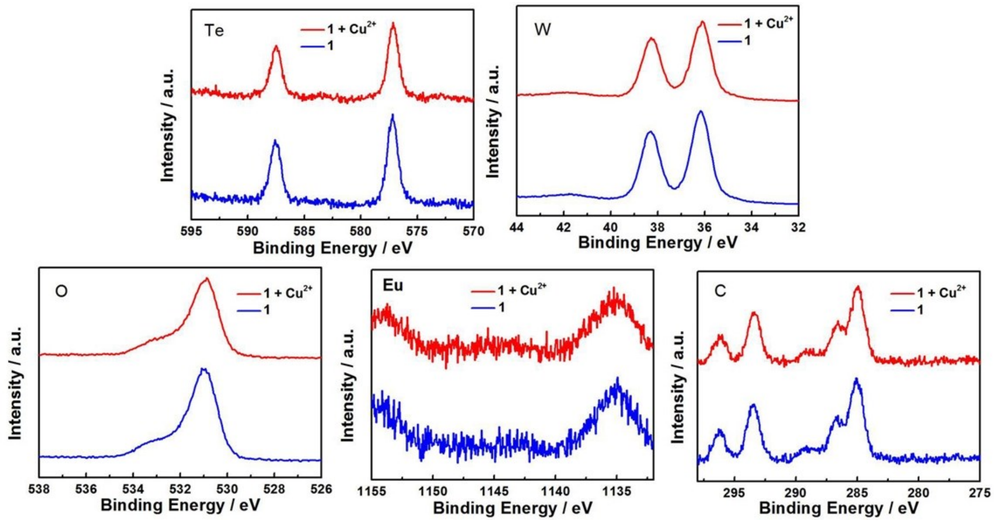

Fig. S21 XPS spectra of the crystals grown in the solutions with and without Cu^{2+} ions.

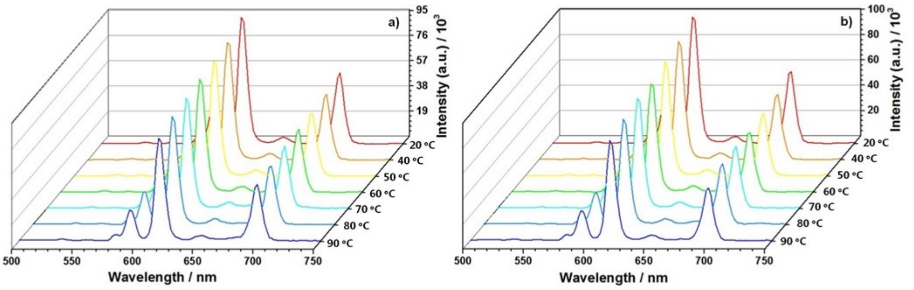

Fig. S22 (a) Emission spectra of the sensor platform in the present of 0.001 mM Cu^{2+} ion in different temperatures (C_1 = 1 mg / mL, λ_{ex} = 394 nm). (b) Emission spectra of the solution of **1** in different temperatures (C_1 = 1 mg / mL, λ_{ex} = 394 nm).

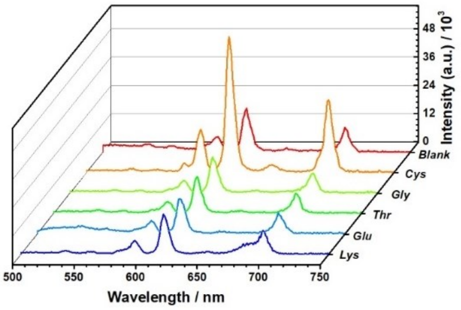

Fig. S23 Evolution of emission spectra for the Cu^{2+}-quenching system based on **1** with addition of different aminoacids. [Conditions: 1.00 mg **1** was added to a series of 1.00 mL solutions simultaneously containing 4.00 $\times 10^{-2}$ mM Cu^{2+} ion and 0.10 mM aminoacids; Aminoacids include polar neutral aminoacid cysteine (Cys), glycine (Gly) and threonine (Thr), polar negative charged aminoacid glutamic acid (Glu), polar positively charged aminoacid lysine (Lys), respectively.]

Fig. S24 ESI–MS spectrum of **1** in aqueous solution and the ESI-MS spectrum of the solution containing **1**, Cu^{2+} and Cys.

References

[1] H. L. Li, Y. J. Liu, J. L. Liu, L. J. Chen, J. W. Zhao and G. Y. Yang, *Chem. Eur. J.*, 2017, **23**, 2673.